Optimization of process parameters for Electroless Ni-Co-P Coating deposition to maximize Micro-hardness

[1]Subhasish Sarkar, [1*]Rishav Kumar Baranwal, [2]Chanchal Biswas, [1]Gautam Majumdar, [3]Julfikar Haider

[1]Department of Mechanical Engineering, Jadavpur University, Kolkata-700032, India

[2]Deartment of Materials and Metallurgical Engineering, Jadavpur University, Kolkata-700032, India

[3]Division of Mechanical Engineering, School of Engineering, Manchester Metropolitan University, Manchester, United Kingdom

**corresponding author*

ABSTRACT

The present study investigates optimisation of microhardness of electroless Ni-Co-P alloy coating over copper substrate. The microhardness of the coating was significantly higher compared to the substrate. Three different design factors i.e., the concentration of cobalt sulphate, concentration of sodium hypophosphite and bath temperatures were used as the process parameters which were optimised by using Box Behnken Design (BBD) and coating micro hardness was taken as a response factor. Vickers' hardness test was conducted to obtain the micro hardness values of the coated samples. From the model analysis results, it was found 15 g/L of cobalt sulphate, 25 g/L of sodium hypophosphite and a bath temperature of 85 °C were the optimum conditions for the coating deposition in order to obtain the hardness value of 1921 HV_{10g}. After annealing at 350 °C the hardness value was further enhanced to 1990 HV_{10g}. Analysis of variance (ANOVA) was carried out to find the graphical relationship between the different process parameters. The detail surface morphology of the Ni-Co-P coating was studied by using an optical microscope and a Scanning Electron Microscope (SEM). The phase and elemental compositions were determined by X-Ray Diffraction (XRD) analysis and Energy Dispersive X-Ray analysis (EDX).

KEYWORDS

electroless coating, Ni-Co-P, Microardness, Box Behnken Design (BBD), ANOVA, Optimisation

1. INTRODUCTION

The electroless nickel coatings were first developed by Brenner and Riddell [1] in 1947. In this coating deposition technique, electron is supplied by a reducing agent instead of electric current, hence the name electroless. The technique is an autocatalytic process in which the substrate is immersed in a solution, the electroless bath, which contains the source of metal ions, reducing agent, bath stabilizer, complexing agent, buffering agent, accelerators, and surfactants or wetting reagents. Nowadays, electroless nickel coating is widely used in many industries [2-4] due to its improved corrosion resistance, wear resistance, magnetic and hardness properties [5-11]. The coating has attracted much attention due to its application in the fields of engineering, surface science, and purification technology used in automotive, chemical and petroleum industries, electronics, food, marine, material handling, pharmaceutical, military, mining, etc. [30]. Ni–Co-P alloy coatings are of huge importance, as they possess high-temperature wear and corrosion resistance characteristics. Moreover, the Ni–Co-P alloy deposition is an anomalous co-deposition and the hardness of alloy increases as long as they possess FCC lattice structure [31]. There are a wide variety of electroless coatings, which can be broadly classified into four categories viz., pure nickel, alloy and poly-alloy coatings, composite coatings and electroless nano coatings. The alloy and poly-alloy coatings can be further classified into binary, ternary and quaternary alloy coatings [12]. In binary alloys, there are two elements in the coating deposition existing in different phases. s. Similarly, in ternary, there are three elements present and in quaternary, there are four elements present [13]. In ternary alloys, an additional element is added to the binary alloys to create a composite or an alloy coating. Literature review suggests that binary coatings like Ni-P and Ni-B has proved to have better tribological and mechanical properties [14-18]. However, the need of having better properties is always a demand in this era and challenging to the researchers at the same time. Hence, the use of a third element/complex like Co, TiO_2, W, Cu, Fe, ZrO_2, Al_2O_3, PTFE, etc. [19-26] is preferred in many cases. Ni-Co-P coating is obtained when cobalt is introduced as an additional element, in order to incorporate the property of electromagnetic shielding, and to improve the anti-corrosion and hardness properties of the surface at the same time [27-29, 43].

The present study focuses on synthesis of Ni-Co-P for increasing the hardness properties of copper substrate and also to find the optimum conditions for obtaining optimized hardness value of the coating. Vickers Hardness Test was used to determine the micro-hardness values of the as-deposited coating. Box Behnken Design (BBD) helped determining the optimum processing conditions. The BBD modelling suggested 17 model values which when compared to the experimental values showed a very slight deviation. Analysis of Variance (ANOVA) was conducted to find out the significant coating deposition parameters and their interactions affecting the hardness of the coating.

2. EXPERIMENTAL DETAILS

2.1. Procedure of Synthesis of the Coating

2.1.1. Substrate Preparation

The substrate material chosen for this experiment was copper, as it is a very readily used material in day-to-day life and has very common but good applications in real life scenarios. The copper substrate was cut from a foil (99.0% pure, lobachemie) which was present in the rolled form. In this experiment, Ni-Co-P coating was deposited on copper substrates of size $20.0\times15.0\times0.1\ mm^3$. After cleaning with distilled water, the substrate was dipped into 3:1 dilute HCl solution for acid pickling in order to remove oxide layer and other foreign metals. Pickling was carried out for 10 minutes followed by cleaning with distilled water. The surfaces of the substrates were activated using palladium chloride solution for 10-15 seconds, which was pre-heated to 55 ^oC. Finally, the substrate was prepared for dipping into electroless bath.

2.1.2. Bath preparation

In bath preparation at first $NiSO_4.6H_2O$, $CoSO_4.7H_2O$, $NaH_2PO_2.H_2O$, $Na_3C_6H_5O_7.2H_2O$ and $(NH_4)_2SO_4$ were taken according to Table 1. The pH Value was maintained at 5. Once the composition was prepared then the substrates were dipped in the electroless bath. Pre-prepared substrates were kept immersed in the bath for an hour to allow the coating to be deposited. After that, the substrates coated with Ni-Co-P were taken out of the bath and rinsed in distilled water. The coating depositions were carried out with different bath compositions and temperatures along with a fixed time, bath volume and pH value. The composition of the bath is given in Table 1.

Table 1: Bath Composition for Ni-Co-P electroless coating deposition

Bath composition	**Quantity**
Nickel sulphate ($NiSO_4.6H_2O$)	25 g/L
Cobalt sulphate ($CoSO_4.7H_2O$)	10/15/20 g/L
Sodium hypophosphite ($NaH_2PO_2.H_2O$)	20/25/30 g/L
Tri-sodium citrate dihydrate ($Na_3C_6H_5O_7.2H_2O$)	15 g/L
Ammonium sulphate ($(NH_4)_2SO_4$)	10 g/L
pH value	5
Time	1 hour
Bath volume	250 cm^3
Bath temperature	80 °C / 85 °C / 90 °C

2.2. Experimental procedure of Micro-Hardness measurement

The coating samples were of dimensions 20.0×15.0×0.1 mm^3. Holding a small piece as such will be difficult in order to perform the hardness test using indentation technique. As a result, the mounting of the coated samples were done using Bakelite as the thermosetting resin. The mounting process was carried out at a temperature and pressure of 175 °C and 240 bar, respectively for 5 minutes. The mounted coated samples underwent Vickers Hardness test aided by an indenter having a diamond tip of 136°. A 10 gram load was applied, and the total time for loading and unloading was allowed to be 15 seconds. Indentation surface area (A) and hardness number (HV) can be calculated by Equation (1) and (2) respectively. The Vickers microhardness Ni-Co-P coated mounted samples were measured as per ASTM standard E384-16 using a hardness tester.

$$A = \frac{d^2}{2\sin\left(\frac{136^0}{2}\right)} \approx \frac{d^2}{1.8544} \quad (1)$$

$$HV = \frac{F}{A} = \frac{1.8544F}{d^2} \quad (2)$$

Where F is the applied load and d is the average diagonal length.

2.3. Design of Experiment through Box Behnken Design (BBD)

The experiment was based on Box Behnken Design to study the combined effects of three independent variables i.e. $CoSO_4$. $7H_2O$ concentration, NaH_2PO_2. H_2O concentration and bath temperature. The independent factor levels were coded as −1 (low), 0 (central point or middle), and 1 (high). Total 17 experiments were conducted with the variation of 3 factors at 3 different levels to fit the experiments in the Box-Behnken modeling (Table 2). Statistical analysis was conducted to optimize the Micro-Hardness of Ni-Co-P Electroless Coating using Design Expert Software [10, 11]. To establish the importance of individual process parameter and their interactions, a regression equation can be formed. It estimates the correlation between the response and the input process parameters.

Table 2: Code and level of Independent Variables

Cobalt sulphate concentration (g/L)		Sodium hypophosphite concentration(g/L)		Bath temperature (°C)	
Code	Level	Code	Level	Code	Level
-1	10	-1	20	-1	80
0	15	0	25	0	85
1	20	1	30	1	90

2.4 Analysis of Variance (ANOVA)

ANOVA was employed to determine the significant parameters that affect the coating microhardness. It uses the concept of p-value and F-value to find the significant factors. The p-value is a parameter by which the null hypothesis can be rejected. If the p-value is less than 0.05, the null hypothesis can be rejected (the parameter is considered as significant). The F-

value is the ratio of the summation of square of the factors to the variance of the errors. Hence, a higher value of F will suggest a relatively better factor with respect to the others.

3. RESULTS AND DISCUSSION

3.1. Hardness Measurements

The hardness of the coated samples was measured and the results are tabulated in Table 3. The hardness obtained by other researchers for Ni-Co-P coating with different coating parameters were just above 1000 VHN_{10g} [32]. The hardness obtained from this experiment showed a variation between 920 and 1956 VHN_{10g}. This was achieved by varying the coating parameters. Hence, in order to maximise the hardness, the optimisation of parameters has proved to be vital.

Table 3: 17 set of experimental variables for the BBD

Set of experiments	Cobalt sulphate ($CoSO_4$) (g/L) (A)	Sodium hypophosphite (NaH_2PO_2) (g/L) (B)	Bath temperature (^{0} C) (C)	Micro Hardness (VHN_{10g})
1	20	20	85	1542
2	20	30	85	955
3	15	25	85	1917
4	10	20	85	920
5	10	25	80	1898
6	10	30	85	1287
7	15	25	85	1921
8	20	25	90	1738

9	15	30	90	923
10	15	25	85	1956
11	15	25	85	1910
12	20	25	80	1084
13	15	20	90	1023
14	15	30	80	1560
15	15	20	80	1353
16	10	25	90	1858
17	15	25	85	1892

The average hardness value of the substrate was measured as 630 HV_{10g}. As the load was applied on the substrate, there being no defined grain boundary, the substrate got penetrated by the indenter, and a lower value of hardness was measured. Hence, a good coating with a defined grain boundary will have better hardness [42]. However, the indentation depth was allowed to be 10% of the coating thickness to avoid the substrates' effect on the hardness.

To get the optimized values of the selected process parameters, Box Behnken Design (BBD) has been used. The BBD is a response surface methodology (RSM) design that requires three levels to run an experiment. Experimental details of Box-Behnken design is given in Table 4. The three different variables are: (i) Concentration of $CoSO_4.7H_2O$ (A), (ii) Concentration of $NaH_2PO_2.H_2O$ (B), and (iii) bath temperatures(C), each of which was assessed at three coded levels lower (−1), middle (0), higher (+1). Average of five hardness values of the same coating is given in the Table 4.

Table 4: Design of experiments based on varying factors

Set of experiments	Cobalt sulphate ($CoSO_4$) (g/L)	Sodium hypophosphite (NaH_2PO_2) (g/L)	Bath temperature (^{0} C)	Micro Hardness (VHN_{10g})
1	+1	-1	0	1542
2	+1	+1	0	955
3	0	0	0	1917
4	-1	-1	0	920
5	-1	0	-1	1898
6	-1	+1	0	1287
7	0	0	0	1921
8	+1	0	+1	1738
9	0	+1	+1	923
10	0	0	0	1956
11	0	0	0	1910
12	+1	0	-1	1084
13	0	-1	+1	1023
14	0	+1	-1	1560
15	0	-1	-1	1353
16	-1	0	+1	1858
17	0	0	0	1892

3.2. Mathematical modeling

3.2.1. Modeling Analysis

The microhardness values obtained from the experiments presented in Table 4 were fed into Design Expert software package to set up mutual relationships between three independent variables according to Equation 3:

$$Y = \beta_0 + \sum_{i=1}^{k} \beta_i X_i + \sum \beta_{ii} X_{ii}^2 + \sum_{i=1}^{k} \sum_{j=2}^{k} \beta_{ij} X_{ij} \quad (3)$$

Where X_1, X_2, and X_3 are the coded values. Therefore the predict response are influenced by coded values and set of regression coefficients: β_0 (intercept coefficients), β_i, β_{ii}, β_{ij}(linear coefficients), β_{11}, β_{22}, β_{33}(quadratic coefficients), β_{12}, β_{13}, β_{23}, β_{123} (interaction coefficients). The model terms were confirmed or declined in terms of the probability (P) value with a 95% confidence level. Using the Design Expert software, the results were completely analyzed via the analysis of variance (ANOVA). Equation 4 and Equation 5 represent the final equations in terms of coded factors and actual factors, respectively.

Final Equation in Terms of Coded Factors:

Micro Hardness = + 1919.20 - 233.50*A + 26.75*B - 241.75*C - 238.50*A*B + 173.50*A*C - 76.75*B*C - 156.72*A^2 - 586.48*B^2 - 117.98*C^2 - 81.75*A^2*B + 395.25A^2C + 306.00*A*B^2 (4)

Final Equation in Terms of Actual Factors:

Micro Hardness = - 48438.47500 - 179.4300*$CoSO_4$ + 1574.17500*NaH_2PO_2 + 766.05500*Temperature - 9.5400*$CoSO_4$*NaH_2PO_2 + 6.94000*$CoSO_4$*Temperature - 3.0700*NaH_2PO_2*Temperature - 6.26900*$(CoSO4)^2$ - 23.45900*$(NaH_2PO_2)^2$ - 4.71900*$(Temperature)^2$ (5)

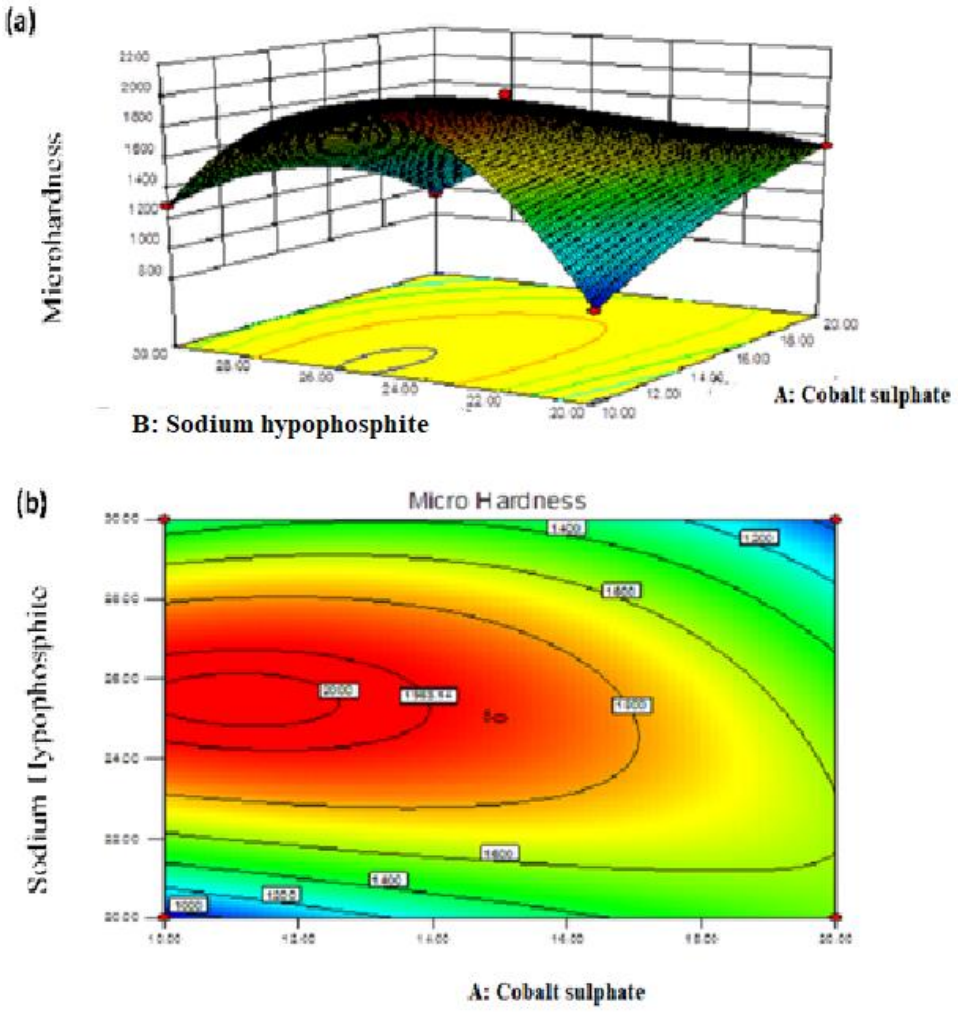

Figure 1: (a) Second-order 3D response surface plot and (b) contour plot to show the variation of micro hardness with cobalt sulphate and sodium hypophosphite concentrations

Figure 1 shows the variation of micro-hardness of the coating with $NaH_2PO_2.H_2O$ and $CoSO_4.7H_2O$. Increasing contours of the plot show the increasing hardness of the coating with the variation in the parameters. The contour height in the descending order are red > yellow > green > blue. The red region corresponds to the region of maximum contour height and hence the maximum hardness. This is the region of optimized values of the parameters. Similarly, Figure 2 shows micro hardness along with the contour plot as a function of concentration of $NaH_2PO_2.H_2O$ and bath temperature. Figure 3 shows micro hardness along with the contour plot as a function of concentration of $CoSO_4.7H_2O$ and bath temperature. Fig. 2 (a) and (b)

shows micro hardness along with the contour plot as a function of concentration of NaH_2PO_2. H_2O and bath temperatures.

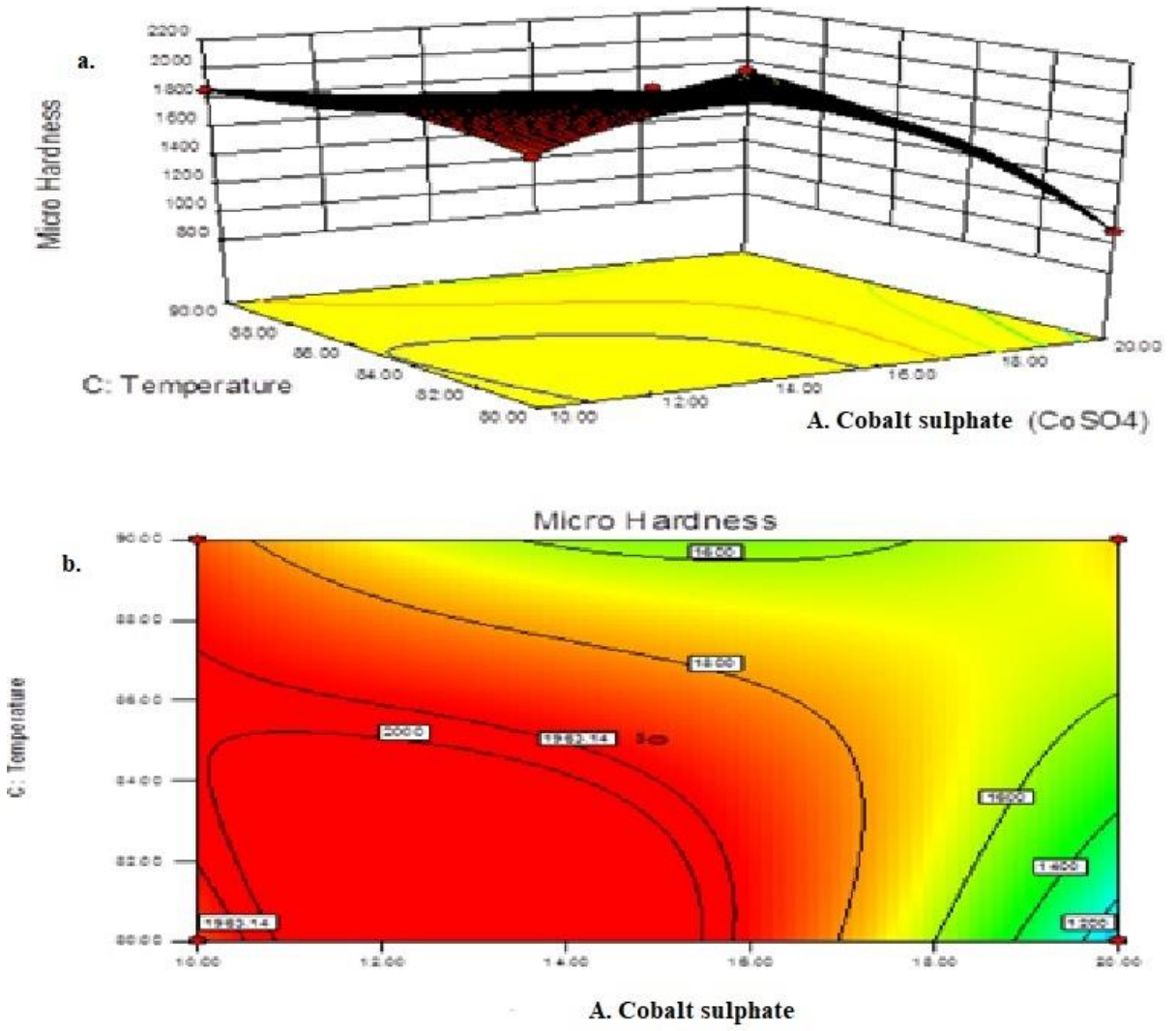

Figure 2: (a) Second-order 3D response surface plot and (b) contour plot to show the variation of micro hardness with cobalt sulphate concentration and bath temperature

322222222

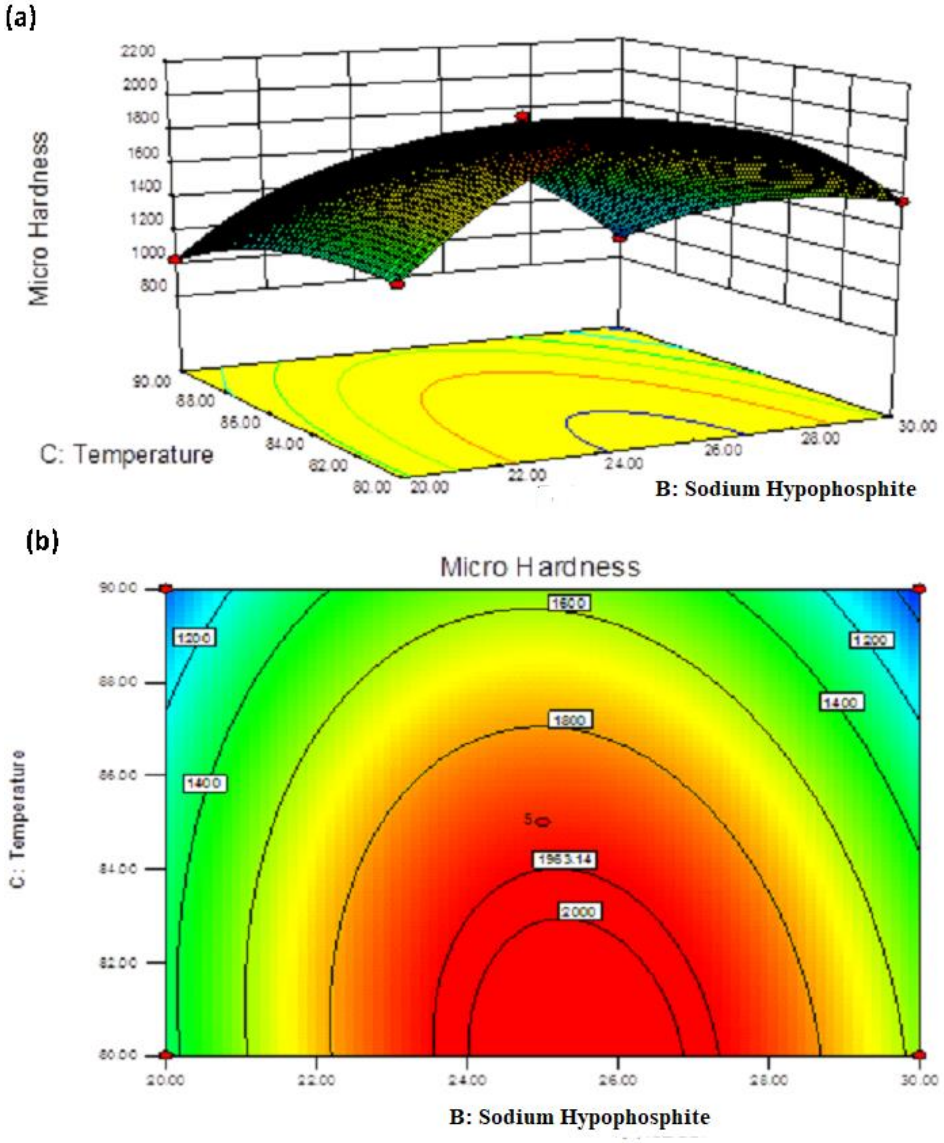

Figure 3: (a) Second-order 3D response surface plot and (a) contour plot to show the variation of micro hardness with sodium hypophosphite concentration and bath temperature

After analysing Figure 1 to Figure 3, the optimisation results of the model for micro hardness of the coated samples are determined and subsequently, the optimised values of the concentration of $CoSO_4$. $7H_2O$ and concentration of NaH_2PO_2. H_2O are found to be 15 g/Land 25 g/L, respectively, along with 85 ^{0} C bath temperature. With these deposition parameters, a

coated sample with a hardness of 1921 HV_{10g} was obtained. This sample further underwent annealing at 350 °C, which offered an increased hardness of 1990 HV_{10g}.

The interaction plot of ANOVA suggests that the interactions $CoSO_4.7H_2O$-Temperature, $NaH_2PO_2.H_2O$-Temperature and $CoSO_4.7H_2O$-$NaH_2PO_2.H_2O$ are very significant in determining the hardness of the optimized coating.

The RS plot in Fig. 1 (A) indicates that the micro hardness rises with an increase in the concentration of $CoSO_4.7H_2O$ and concentration of $NaH_2PO_2.H_2O$. Fig. 2(A) shows that micro hardness increases with the concentration of $CoSO_4.7H_2O$ but the maximum value is achieved at 85 ^{0} C. Fig. 3 (A) shows that micro hardness increases with the concentration of $NaH_2PO_2.H_2O$ and the maximum value is achieved at 85 $^{\circ}$C bath temperature. Comparing the contour plots in Fig. 1 (B), 2 (B) and 3 (B), it can be inferred that the concentration of $CoSO_4.7H_2O$ and the concentration of $NaH_2PO_2.H_2O$ have more influence on the micro hardness than the bath temperature. However, it can be concluded that the concentration of $CoSO_4.7H_2O$, is a significant factor in determining the micro-hardness of the coating. The interaction between concentration of $CoSO_4.7H_2O$ and bath temperature also stand significant.

The analysis of results of ANOVA for response surface quadratic models representing hardness of electroless coating is presented in Table 5. It shows that the model F-value is 405.13, implying that the model is significant. There is only a 0.01% chance that such high F-value could occur due to noise. The values of the model with Prob> F is less than 0.0500, indicating that the model terms are significant [41]. In this case, A, B, C, AB, BC, A2, B2 and C2 are significant model terms. As per the table value, R^2 of 0.9992 is in reasonable agreement with the Adj R^2 of 0.9967 i.e. the difference is less than 0.1. Adequate precision measures the signal to noise ratio which should ideally be greater than 4. Our study exhibits a ratio of 48.869 indicating adequate signal. This model can be used to navigate the design space. The coefficient of variance (CV) for micro hardness is calculated to be 1.54. Consideration of the values of all the parameter of ANOVA statistical results of the model are found to be significant in this work. The model performed 17 batch runs as shown in Table 4 by using the Design Expert 9 software and it followed second-order quadratic equations (3) and (4) to calculate the hardness of the coated samples. Solved simultaneously, the equations determine F-value of the significance of individual coefficient. Higher significance of the model indicates smaller F-values. The values including the independent variables A, B, C and the interacting variables AB, AC, BC as well as quadratic variables A2, B2, C2, are significant. The interactions

between the factors can be interpreted from Figures 1 to 3. If no intersection occurs between the plots then it states that no significant interaction has taken place. However, a steeper graph with intersection points suggests significant interactions took place between the factors.

Table 5: Shows results of the BBD model

Statistical results of the ANOVA	
Model F Value	405.13
Std. Dev.	23.38
Mean	1513.94
C.V. %	1.54
R-Squared	0.9992
Adj R-Squared	0.9967
Adeq Precision	48.869

3.2.2 Comparison of the experimental and model value, and analysis:

The experimental and model values of hardness are recorded and presented in Table 6. The model values were calculated with Equation 4.

Table 6: Analysis of experimental value with model value

Set of experiments	Experimental values	Model values	Error in percentage
1	1542	1348.125	1.94
2	955	842.875	1.12
3	1917	1919.2	-0.02

4	920	1032.125	-1.12
5	1898	1942.625	-0.45
6	1287	1657.275	-3.70
7	1921	1919.2	0.02
8	1738	1693.375	0.45
9	923	1079.75	-1.57
10	1956	1919.2	0.37
11	1910	1919.2	-0.09
12	1084	1434.625	-3.51
13	1023	1261.5	-2.39
14	1560	1321.5	2.39
15	1353	1196.25	1.57
16	1858	1507.375	3.51
17	1892	1919.2	-0.27

The deviation of the experimental results from the model values is found to be less than 4%. Hence, it can be concluded from the results that the experimental values match the model values with a high degree of similarity. Graphical analysis of the experimental values and the model hardness values for the set of experiments has been presented in Figure 4.

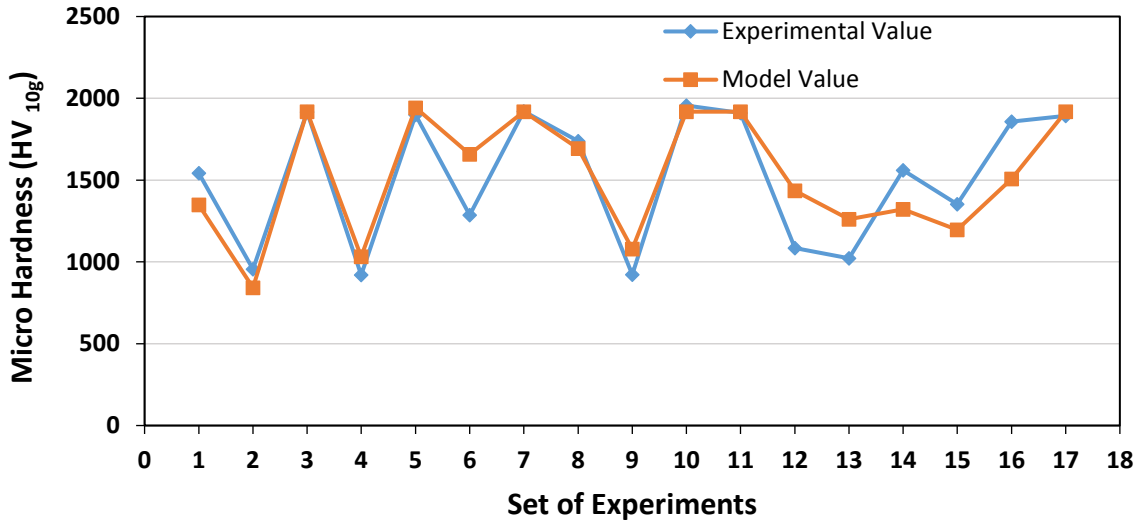

Figure 4: Graphical analysis of experimental and model hardness values

3.3 XRD analysis of copper substrate and as-deposited Optimised Coated Sample

Phase analysis was carried out by the X-ray diffraction method in a RigakuUltima-III machine, using Cu Kα radiation with 2θ in the range from 20° to 80° with a scan speed of 2° min^{-1}. X-ray diffraction studies of the copper substrate confirmed the routine diffractogram of (FCC) copper and it showed only copper phase prominently (Figure 5). XRD analysis of the as-prepared Ni-Co-P coating shows the presence of Ni_3P, CoP_2, and NiP_3 phases as evidenced in Figure 6.

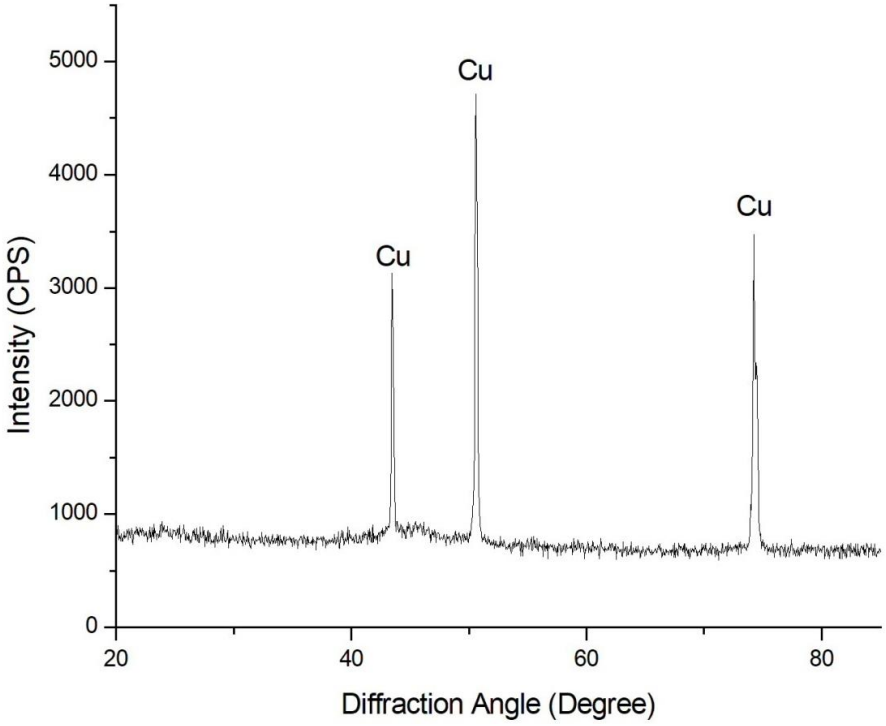

Figure 5: X-ray diffraction pattern of the copper substrate

Farr and Noshani [32] showed the presence of Co_2P phase as minor peaks in the XRD pattern in the as-deposited Ni-Co-P coating. The presence of sharp peaks, in this case, indicated that the deposits had some crystallized forms present in the coating. In addition to these peaks, stable peaks of Ni_3P phase were observed with NiP_3 phase as well which was also observed by other researchers in hypereutectic Ni coatings (phosphorus percentage greater than 11%) [33-35]. The presence of the Ni_3P phase in the coating increases the hardness of the coating because of the crystalline form and the ability of the crystalline form to withstand more stress before grain deformation than that of the amorphous deposits [36-39].

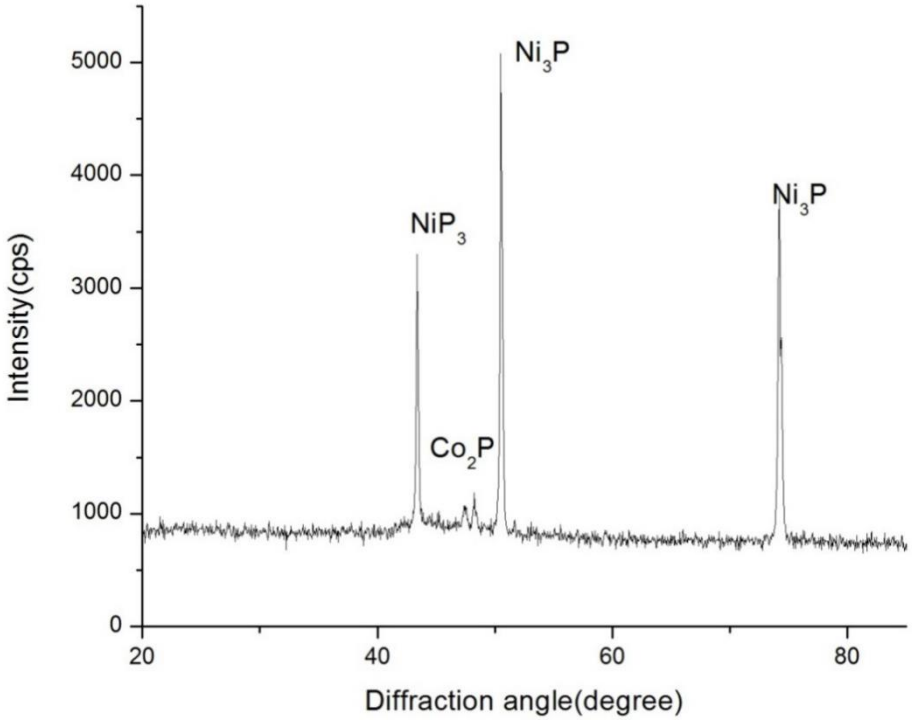

Figure 6: XRD plot of the optimised Ni-Co-P coated Sample

3.4. SEM and EDX analysis

3.4.1. Analysis of substrate

The copper samples after being cleaned using acid pickling, rinsed with water and dried was analysed using a Scanning Electron Microscope (SEM) and an Optical Microscope. Images of the copper substrate etched with ferric chloride ($FeCl_3$) have been presented in Figure 7. to observe the surface morphology. The SEM analysis was performed with SOF software, installed in a JEOL-Jsm 7610F machine. Elongated grains of the substrate were observed with no defined grain boundary.

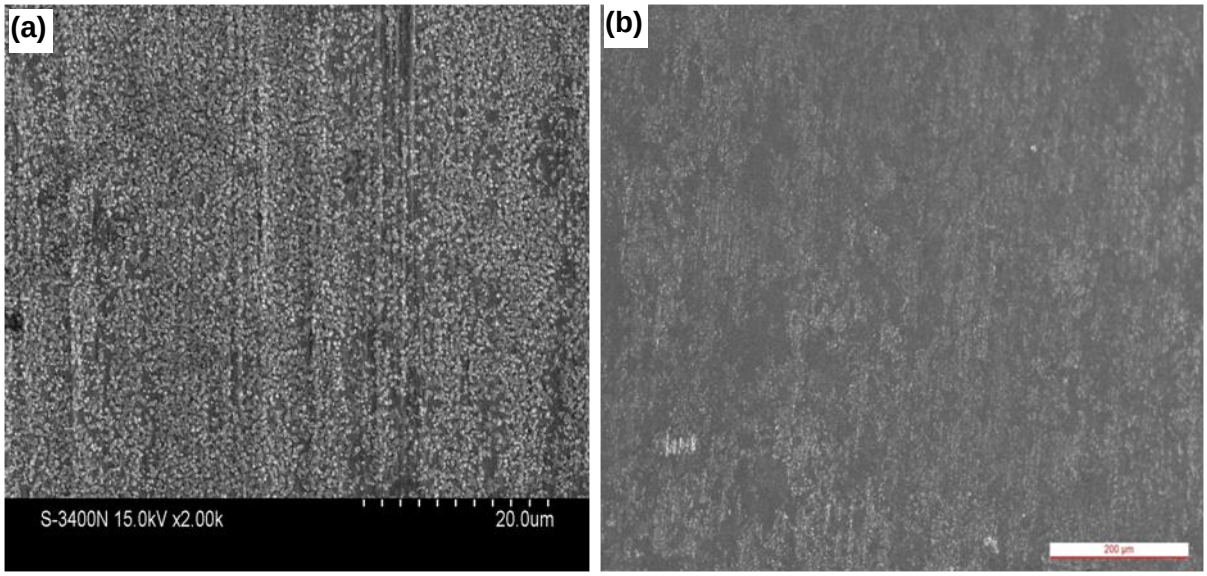

Figure 7. (a) SEM of the copper Substrate without etching (b) Optical Microscopy Image of copper substrate with ferric chloride ($FeCl_3$) etching

3.4.2. Analysis of optimized coated sample

Figure 8 (a) shows granular type structures distributed over the surface of the coated sample. Figure 8 (b) shows the SEM micrograph of the optimised as-deposited Ni-Co-P coated sample with granular grain structure whereas Figure 8 (c) shows the surface of the annealed sample revealing the growth or spreading of the metallic phosphides. The deposited layer became more diffused with swelling of the metallic compounds.

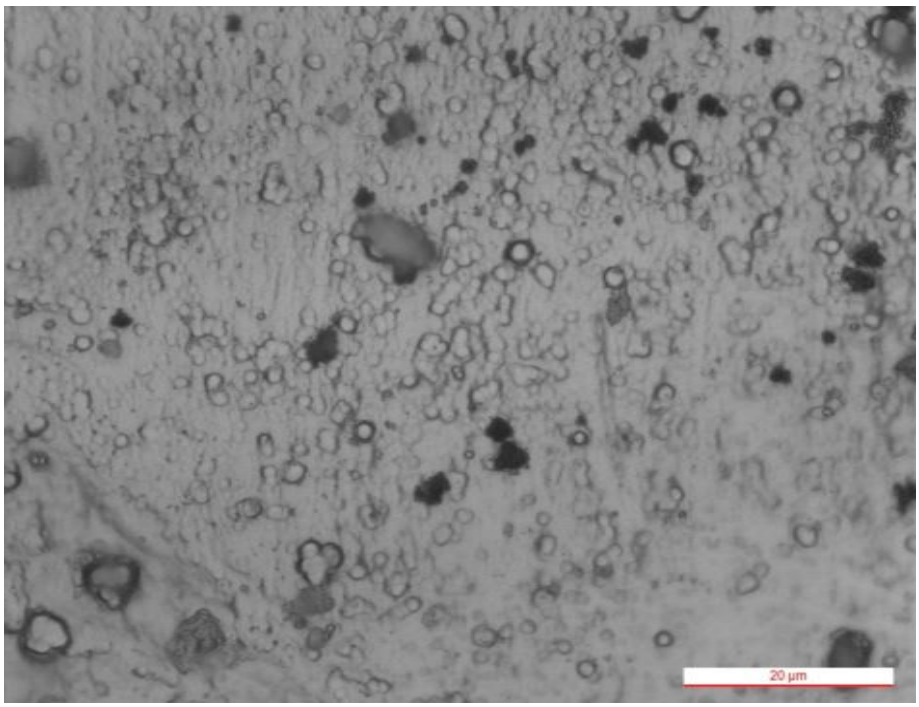

Figure 8: (a) Optical Microscopy of optimised sample with dilute HCl and $FeCl_3$ etching

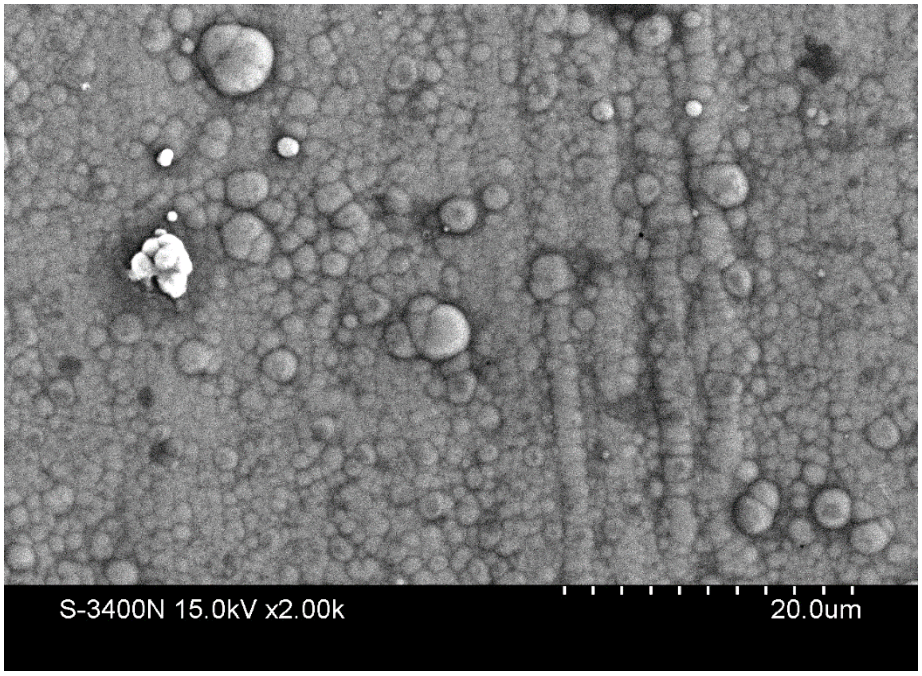

Figure 8: (b) SEM Micrograph of the as-deposited optimised sample

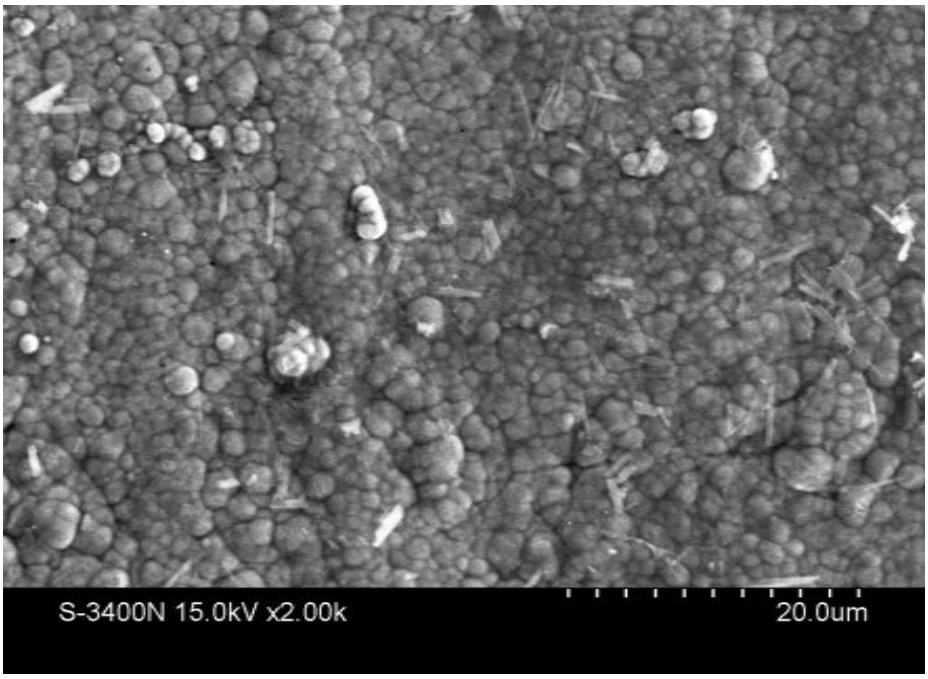

Figure 8: (c) SEM Micrograph of annealed optimised sample

3.4.3. Chemical composition of the electroless coating

Energy Dispersive X-Ray (EDX) spectroscopy was carried out with AZTEC software connected to OXFORD X-max 50 machine, to find out the weight percentage of different

elements present in the coating. The corresponding EDX analysis is shown in Figure 9, which indicates the presence of elemental Ni, Co and P.

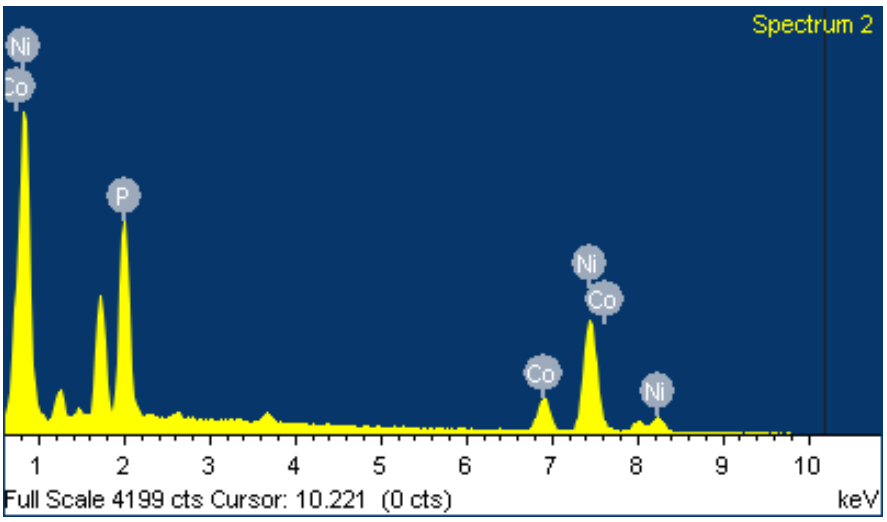

Figure 9: EDX analysis of optimized Ni-Co-P coating

Table 7 lists the weight percentages of the individual elements in the optimized coated sample. Percentage of cobalt is much less compared to that of nickel, which indicates that the Ni-P being the basic coating with cobalt being used as an alloying component. The atom size of nickel and cobalt is same (200 pm) with phosphorus (195 pm) being smaller than the other two. Therefore, the smaller phosphorus atoms present in the Ni-Co-P coating occupies those spaces where compressive stresses are present [40]. The presence of the smaller atoms in the matrix (phosphorus in this case) induces tensile stress, thus nullifying the stresses and reducing the overall internal stresses within the coating. This phenomenon can support the observation of sharp peak in the XRD analysis of the coating [36].

Table 7: Weight percentage of elements present in the coating

Element	Weight Percentage (wt%)
Nickel	66.58
Cobalt	15.68

Phosphorus	17.74
Total	100.00

CONCLUSIONS

This investigation has provided a strong feasibility of electroless ternary constituents' coating deposition (Ni-Co-P) on copper substrate. From the experimental data and the optimization process parameters, it can be concluded that 15 g/L of $CoSO_4.7H_2O$, 25 g/L of $NaH_2PO_2.H_2O$ and 85 °C bath temperature were the optimum conditions to achieve a Ni-Co-P coating with a microhardness of 1956 HV_{10g}. After annealing the hardness value increased to 1990 HV_{10g}, whereas copper substrate hardness was only 630 HV_{10g}. It was clearly seen that comparing the hardness of the optimized sample and the substrate without coating there is a massive enhancement in hardness. The percentage increase in hardness from substrate to the as-deposited coated sample was 205% and substrate to the as deposited annealed coated sample was 216%. ANOVA results showed that cobalt sulphate concentration and all the interactions were significant in determining the hardness of the coating. SEM analysis revealed granular grains of the coating while XRD showed the presence of three phases (Ni_3P, CoP_2 and NiP_3) and EDX showed the highest concentration of the cobalt and phosphorus in the coating. The deviation of the experimental hardness values from the modelling values was in the range of -3.71% to +3.51%, which was a very minute value. Therefore, it can be concluded that the optimized modelling value and the experimental value are almost identical, thus proving this modelling to be cost effective and time saving simultaneously. The developed model can be used to predict micro-hardness of the electroless Ni-Co-P coating in industrial applications without conducting extensive experimental trials.

REFERENCES

1. Brenner A, Riddell GE(1947) Deposition of nickel and cobalt by chemical reduction. J. Res. Nat. Bur. Stand. 39:385-95.

2. Shu X, Wang Y, Peng J, Yan P, Yan B, Fang X, Xu Y(2015) Recent progress in electroless Ni coatings for magnesium alloys. Int J Electrochem Sci. 10:1261-73.

3. Wang C, Farhat Z, Jarjoura G, Hassan MK, Abdullah AM (2017) Indentation and erosion behavior of electroless Ni-P coating on pipeline steel. Wear. 376:1630-9.

4. Loto CA (2016) Electroless nickel plating–a review. Silicon. 8(2):177-86.

5. M.Rezagholizadeha, M. Ghaderia, A. Heidarya, and S.M.M. Vaghefib.Electroless Ni–P/Ni–B–B_4C (2014) Duplex Composite Coatingsfor Improving the Corrosion and TribologicalBehavior of Ck45 Steel ISSN 2070_2051. Protection of Metals and Physical Chemistry of Surfaces 51(2): 234–239.

6. Gu C, Lian J, Li G, Niu L, Jiang Z. (2005) Electroless Ni–P plating on AZ91D magnesium alloy from a sulfate solution. Journal of Alloys and Compounds. 391(1-2):104-9.

7.Valova E, Georgieva J, Armyanov S, Avramova I, Dille J, Kubova O, Delplancke-OgletreeM-P (2010) Corrosion behavior of hybrid coatings: Electroless Ni–Cu–P and sputtered TiN. Surface & Coatings Technology 204:2775–2781.

8.Gao Y, Huang L, Zheng ZH, Li H, Zhu M (2007) The influence of cobalt on the corrosion resistance and electromagnetic shielding of electroless Ni–Co–P deposits on Al substrate. Applied Surface Science 253:9470–9475.

9.Farajia S, Rahim AA, Mohamed N,Sipaut CS, Raja B (2013) Corrosion resistance of electroless Cu–P and Cu–P–SiC composite coatings in 3.5% NaCl. Arabian Journal of Chemistry 6, 379–388.

10.Delaunois F, Petitjean JP, Lienard P, Jacob-Duliere M (2000) Autocatalytic electroless nickel-boron plating on light alloys. Surface and Coatings Technology. 124(2-3):201-9.

11.Lee CK. Corrosion and wear-corrosion resistance properties of electroless Ni–P coatings on GFRP composite in wind turbine blades. (2008) Surface and Coatings Technology. 202(19):4868-74.

12.Sudagar J, Lian J, Sha W. (2013) Electroless nickel, alloy, composite and nano coatings – A critical review.Journal of Alloys and Compounds 571:183–204.

13.Sahoo P, Das SK (2010) Tribology of electroless nickel coatings - A review.

14. Zhai T, Liu B, Ding CH, Lu LX, Zhang C, Xue KG, Yang DA. (2015) Ni–P electroless deposition directly induced by sodium borohydride at interconnected pores of poly (ether ether ketone)/multiwalled carbon nanotubes composites surface. Surface and Coatings Technology. 272:141-8.

15.Sano M, Tahara Y, Chen CY, Chang TF, Hashimoto T, Kurosu H, Sato T, Sone M. (2016) Application of supercritical carbon dioxide in catalyzation and Ni-P electroless plating of nylon 6, 6 textile. Surface and Coatings Technology. 302:336-43.

16. Rajabalizadeh Z, Seifzadeh D (2017) Application of electroless Ni-P coating on magnesium alloy via CrO3/HF free titanate pretreatment. Applied Surface Science. 422:696-709.

17. Wen XP, Dai HB, Wu LS, Wang P (2017) Electroless plating of Ni–B film as a binder-free highly efficient electrocatalyst for hydrazine oxidation. Applied Surface Science. 409:132-9.

18. Eraslan S, Ürgen M (2015) Oxidation behavior of electroless Ni–P, Ni–B and Ni–W–B coatings deposited on steel substrates. Surface and Coatings Technology. 265:46-52.

19. Yan Y, Tian Y, Hao M, Miao Y (2016) Synthesis and characterization of cross-like Ni-Co-P microcomposites. Materials & Design. 111:230-8.

20. Liu J, Wang X, Tian Z, Yuan M, Ma X (2015) Effect of copper content on the properties of electroless Ni–Cu–P coatings prepared on magnesium alloys. Applied Surface Science. 356:289-93.

21. Karthikeyan S, Ramamoorthy B (2014) Effect of reducing agent and nano Al_2O_3 particles on the properties of electroless Ni–P coating. Applied Surface Science.307:654-60.

22. Lee HB, Wu MY (2017) A Study on the Corrosion and Wear Behavior of Electrodeposited Ni-WP Coating. Metallurgical and Materials Transactions A. 48(10):4667-80.

23. Liew KW, Kong HJ, Low KO, Kok CK, Lee D (2014) The effect of heat treatment duration on mechanical and tribological characteristics of Ni–P–PTFE coating on low carbon high tensile steel. Materials & Design. 62:430-42.

24. An Z, Zhang X, Li H (2015) A preliminary study of the preparation and characterization of shielding fabric coated by electrical deposition of amorphous Ni–Fe–P alloy.Journal of Alloys and Compounds. 621:99-103.

25. Shu X, Wang Y, Liu C, Aljaafari A, Gao W. (2015) Double-layered Ni-P/Ni-P-ZrO2 electroless coatings on AZ31 magnesium alloy with improved corrosion resistance. Surface and Coatings Technology. 261:161-6.

26. Wu X, Mao J, Zhang Z, Che Y (2015) Improving the properties of 211Z Al alloy by enhanced electroless Ni–P–TiO2 nanocomposite coatings with TiO2 sol. Surface and Coatings Technology. 270:170-4.

27. Narayanan TS, Selvakumar S, Stephen A (2003) Electroless Ni–Co–P ternary alloy deposits: preparation and characteristics. Surface and Coatings Technology.172(2-3):298-307.

28.Gao Y, Huang L, Zheng ZJ, Li H, Zhu M (2007) The influence of cobalt on the corrosion resistance and electromagnetic shielding of electroless Ni–Co–P deposits on Al substrate. Applied Surface Science. 253(24):9470-9475.

29. Seifzadeh D, Hollagh AR (2014) Corrosion resistance enhancement of AZ91D magnesium alloy by electroless Ni-Co-P coating and Ni-Co-P-SiO 2 nanocomposite. Journal of materials engineering and performance. 23(11):4109-4121.

30.Tamilarasan TR, Rajendran R, Siva Shankar M, Sanjith U, Rajagopal G, Sudagar J (2016) Wear and scratch behaviour of electroless Ni-P-nano-TiO2: Effect of surfactants. Wear 346–347:148-157.

31.Li Y, Wang R, Qi F,Wang C (2008) Preparation, characterization and microwave absorption properties of electroless Ni–Co–P-coated SiC powder. Applied Surface Science. 254 (15): 4708-4715.

32. Farr JP, Noshani AA (1996) Some properties of electroless Ni-P, Co-P, and Ni-Co-P deposits. Transactions of the IMF. 74(6):221-5.

33. Aal AA, Shaaban A, Hamid ZA (2008) Nanocrystalline soft ferromagnetic Ni–Co–P thin film on Al alloy by low temperature electroless deposition. Applied Surface Science. 254(7):1966-71.

34. Younan MM, Aly IH, Nageeb MT (2002) Effect of heat treatment on electroless ternary nickel–cobalt–phosphorus alloy. Journal of Applied Electrochemistry. 32(4):439-46.

35. Tsai YY, Wu FB, Chen YI, Peng PJ, Duh JG, Tsai SY (2001) Thermal stability and mechanical properties of Ni–W–P electroless deposits. Surface and Coatings Technology. 2001 146:502-7.

36. Keong KG, Sha W, Malinov S (2003) Hardness evolution of electroless nickel–phosphorus deposits with thermal processing. Surface and Coatings Technology. 168(2-3):263-74.

37. Zhang YZ, Wu YY, Yao M (1998) Characterization of electroless nickel with low phosphorus. Journal of materials science letters. 17(1):37-40.

38. Sui ML, Lu K (1994) Variation in lattice parameters with grain size of a nanophase Ni3P compound. Materials Science and Engineering: A. 179:541-4.

39. Park SH, Lee DN (1998) A study on the microstructure and phase transformation of electroless nickel deposits. Journal of Materials Science. 23(5):1643-54.

40. Callister WD, Rethwisch DG. Materials science and engineering. NY: John Wiley & Sons; 2011.

41. Altman DG, Bland JM (1995) Statistics notes: Absence of evidence is not evidence of absence. Bmj. 311(7003):485.

42. Biswas N, Baranwal RK, Majumdar G, Brabazon D (2018) Review of duplex electroless coatings and their properties. Advances in Materials and Processing Technologies. 28:1-8.

43. Sarkar S, Baranwal RK, Lamichaney S, De J, Majumdar G (2018) Optimization of electroless Ni-Co-P coating with hardness as response parameter: A computational approach. Jurnal Tribologi. 18:81-96.